

Supporting Information for

Unleashing the Power of the Sun: The Increasing Impact of the Solar Cycle on Off-Season Super Typhoons since the 1990s

Chau-Ron Wu^{1,*}, Yong-Fu Lin², I-I Lin³, and Jin-Yi Yu^{2,*}

¹Department of Earth Sciences, National Taiwan Normal University, Taipei, Taiwan

²Department of Earth System Science, University of California, Irvine, CA, USA

³Department of Atmospheric Sciences, National Taiwan University, Taipei, Taiwan

*Correspondence to jyyu@uci.edu, cwu@ntnu.edu.tw

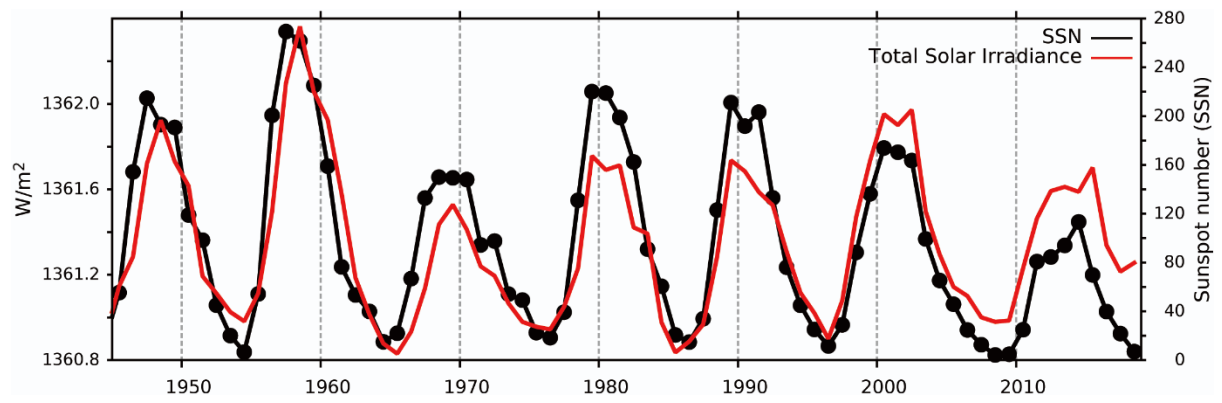
This PDF file includes:

Supplementary Table 1

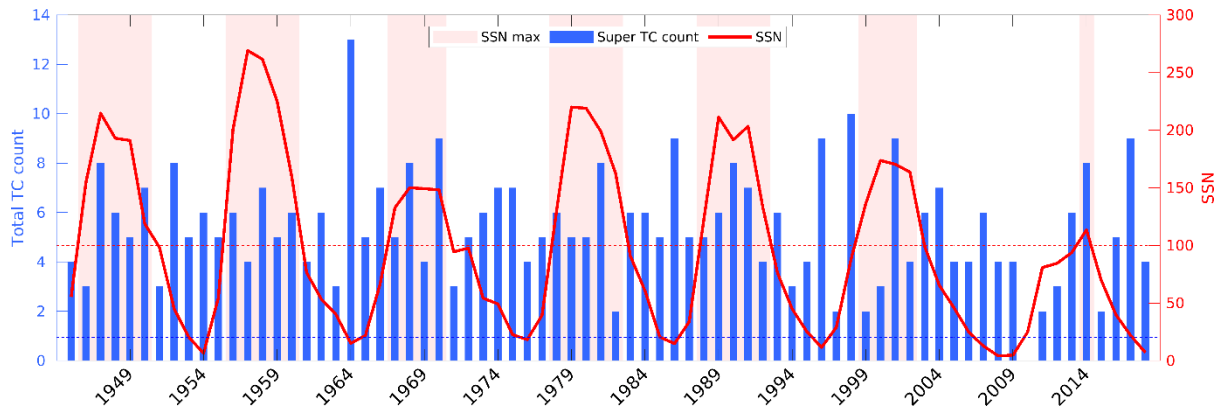
Supplementary Figures 1-15

Supplementary Table 1. Correlation coefficients between SSN and super typhoon numbers (STN) with a one-year lag were calculated for the periods 1945-2018 and 1985-2018 (top row). Additionally, the table presents the same one-year lag correlations, computed after eliminating the influences of ENSO through a 7-year running mean, and removing the effects of PDO and AMO using linear regression methods, all from the STN time series (second and third rows).

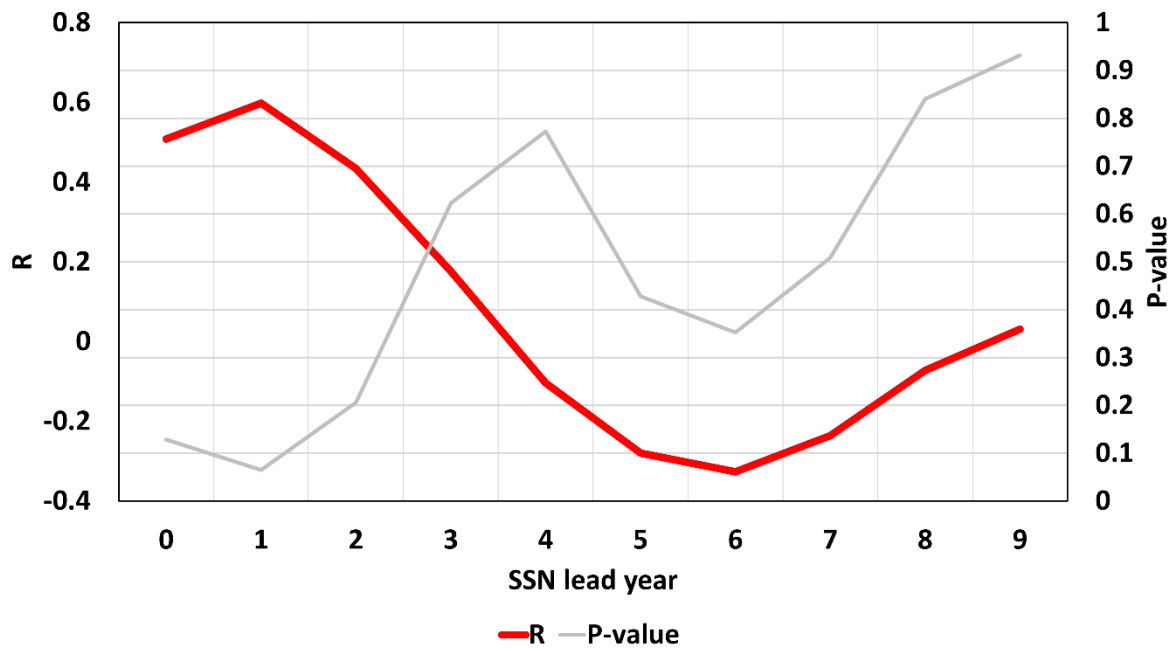
SSN leads one year	Correlation coefficient (1945-2018)	Correlation coefficient (1985-2018)
SSN vs STN	0.26 (P=0.22)	0.6 (P<0.1)
SSN vs STN (remove AMO)	0.21 (P=0.32)	0.58 (P<0.1)
SSN vs STN (remove PDO)	0.22 (P=0.30)	0.51 (P<0.1)



Supplementary Figure 1. Time series of yearly sunspot number (SSN, red line) and total solar irradiance (TSI, black line) during the period 1945-2018.

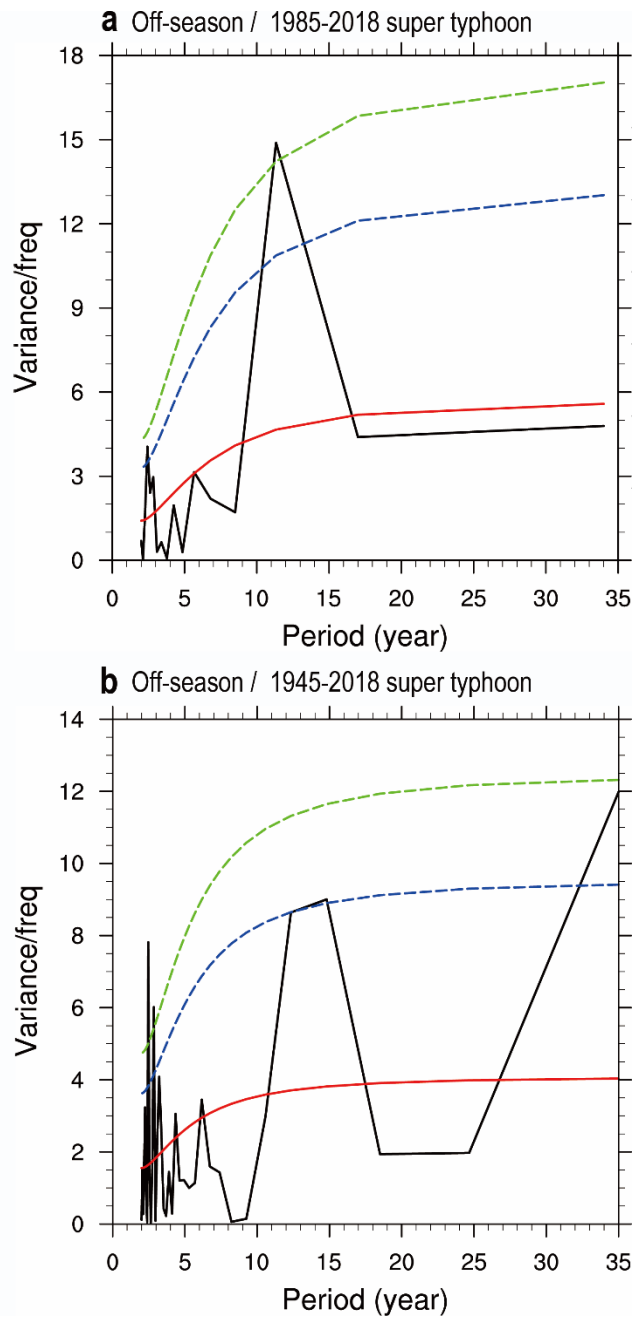


Supplementary Figure 2. The time series plot displays the yearly (January-December) SSN numbers (red line) and the number of total off-season typhoons (blue bars) in the western North Pacific during the period 1945-2018. The red and blue-dashed lines denote the thresholds used to define SSNmax (SSN \geq 100, active) and SSNmin (SSN \leq 20; inactive) periods of the solar cycle, respectively. The active periods are shaded pink.



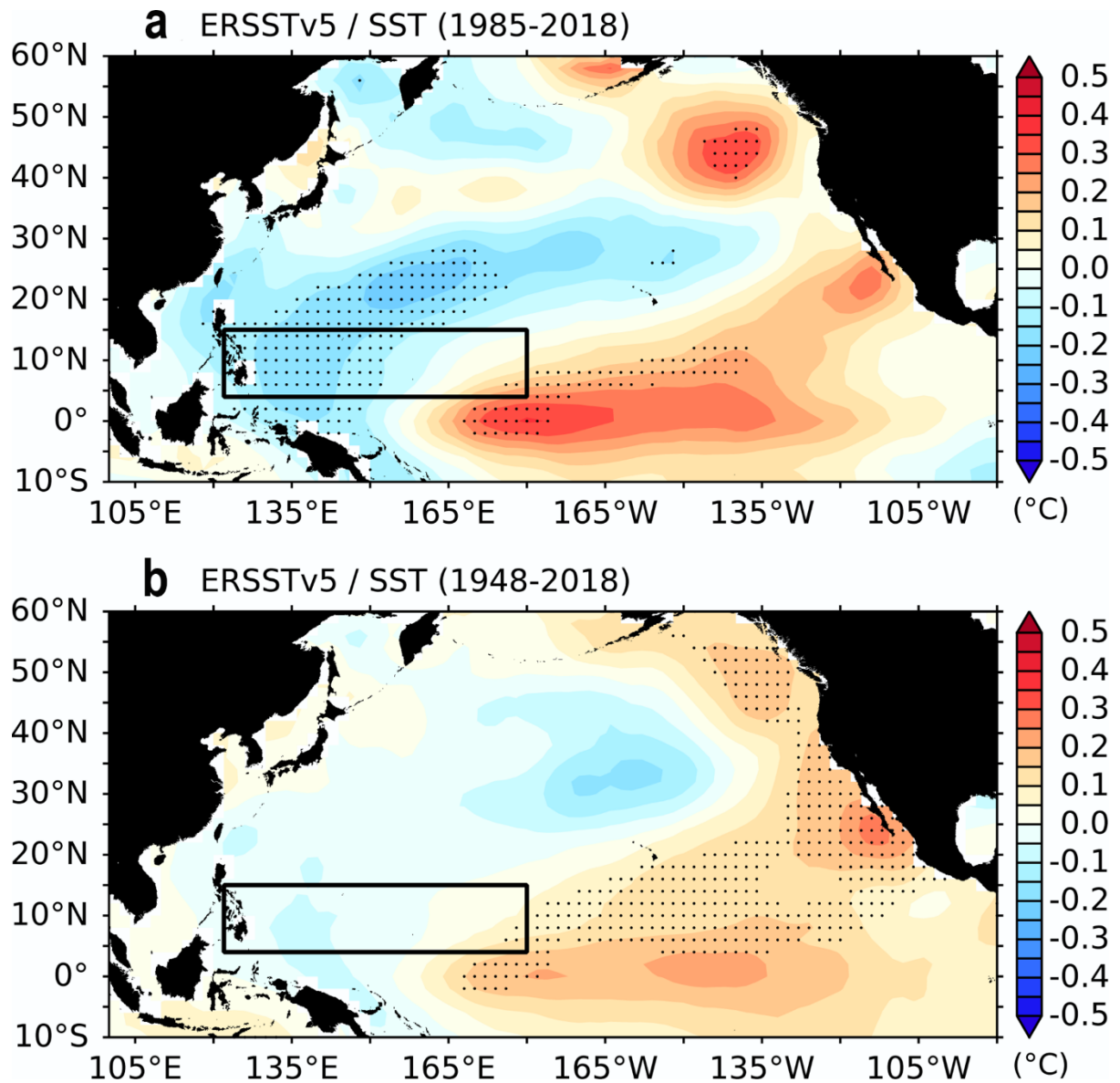
Supplementary Figure 3. Lag correlation between the yearly number of SSN and off-season super typhoons in the western North Pacific during the period 1985-2018.

The red line and gray lines indicate the correlation coefficient and P-value, respectively, when the yearly number of off-season (boreal winter and spring) lags the yearly SSN.



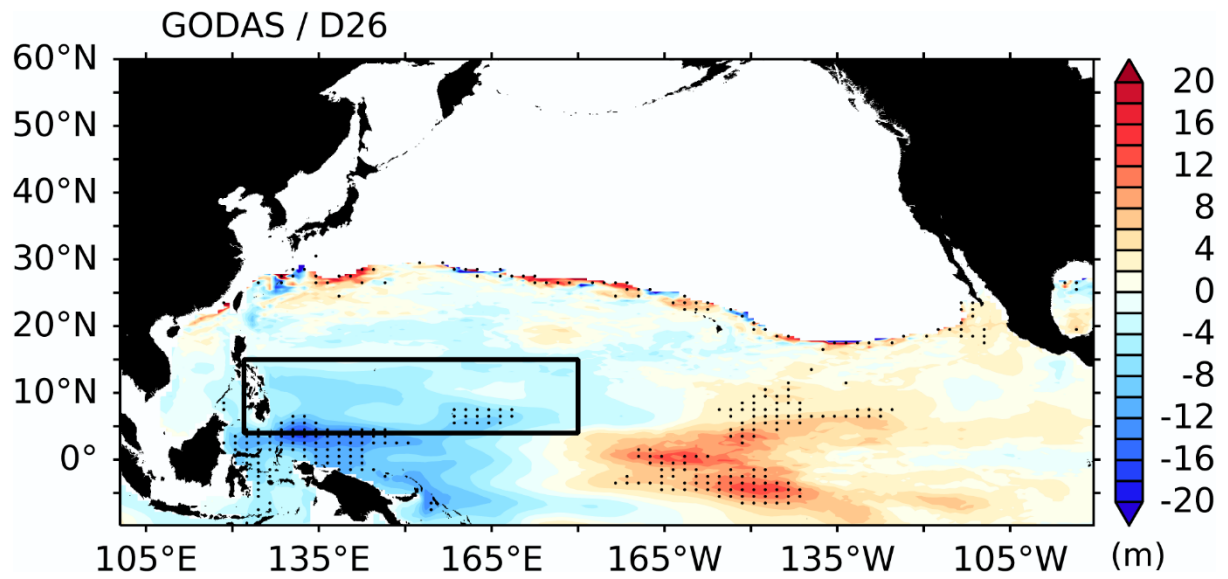
Supplementary Figure 4. Power spectrum of the yearly number of off-season (November-April) super typhoons in the western North Pacific.

(a) The spectrum calculated for the period of strongest modulation (1985-2018). (b) The same calculation as (a), but for the entire analysis period (1945-2018). The red lines represent the theoretical Markov red noise spectrum, and its significance is indicated by the blue (90th percentile) and green (95th percentile) dashed lines.



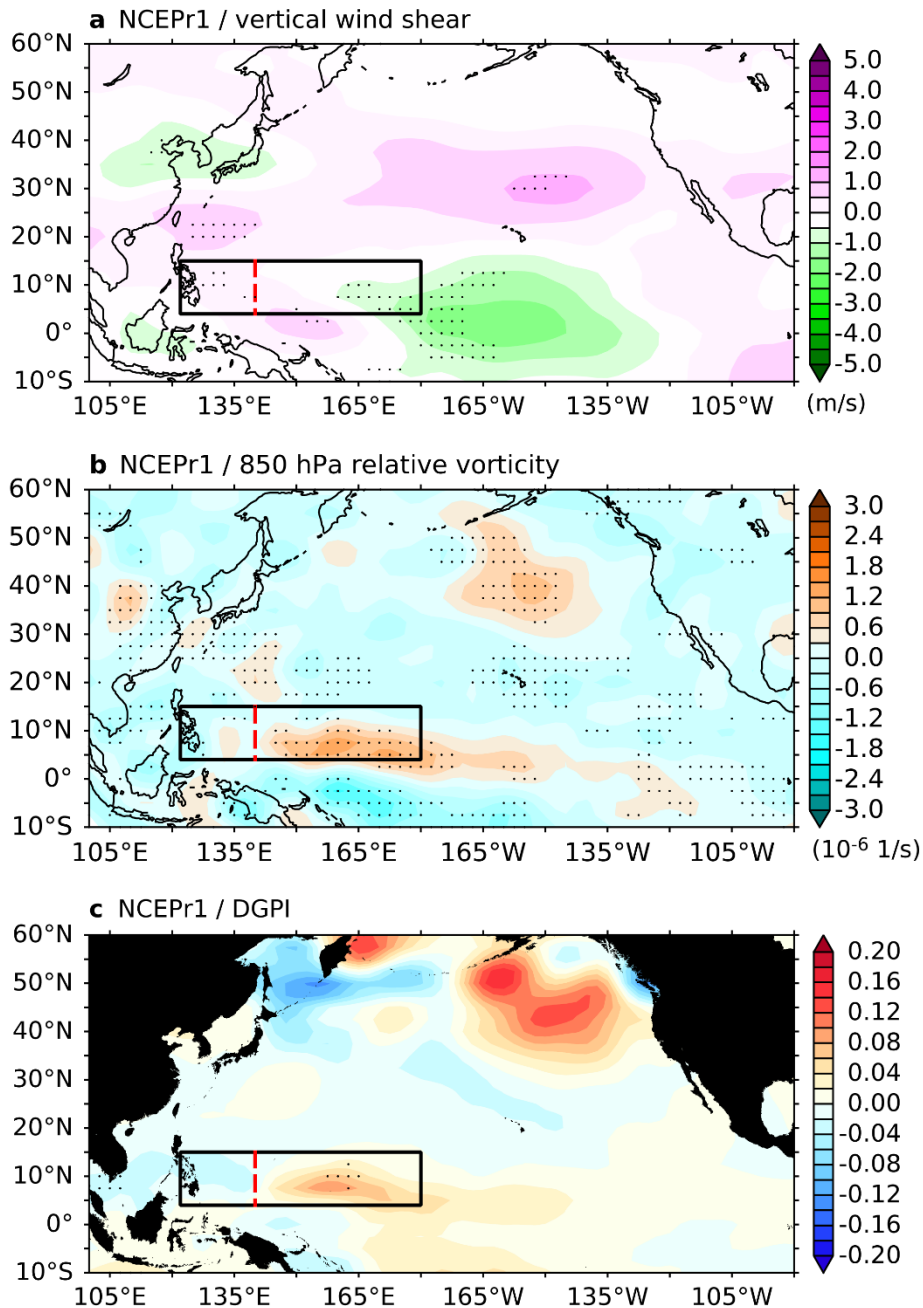
Supplementary Figure 5. Pacific sea surface temperature (SST) response to the solar cycle.

(a) Regression of off-season (November-April) Sea Surface Temperature (SST) onto the yearly normalized sunspot number (SSN) with a one-year lag (i.e. SSN leads by one year) during the period 1985-2018. The colors indicate the SST values (unit in °C). (b) The same regression, but for the period 1948-2018. The stippled areas indicate regions where the regressions are significant at the 90% confidence level, determined using a Student's t-test. The black box represents the OMDR.



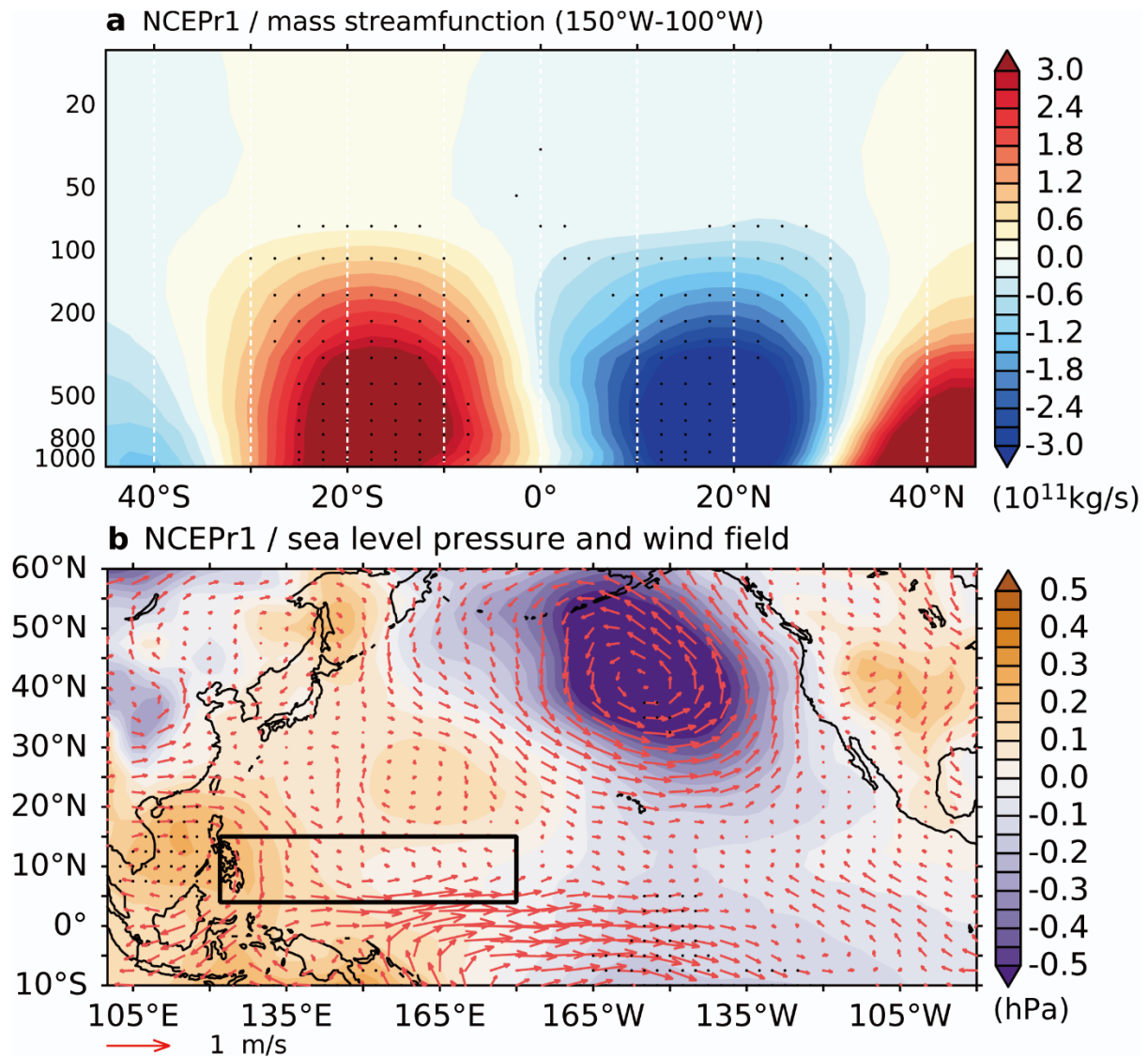
Supplementary Figure 6. The response in the depth of the 26°C isotherm (D26) in the North Pacific to the solar cycle.

Regressions of off-season (November-April) D26 (colors, unit in m) onto the yearly normalized SSN at a one-year lag (i.e., SSN leads by one year) during the period 1985-2018. The stippled areas indicate where the regressions are significant at the 90% confidence level determined using a Student's t-test. The black box indicates the OMDR.



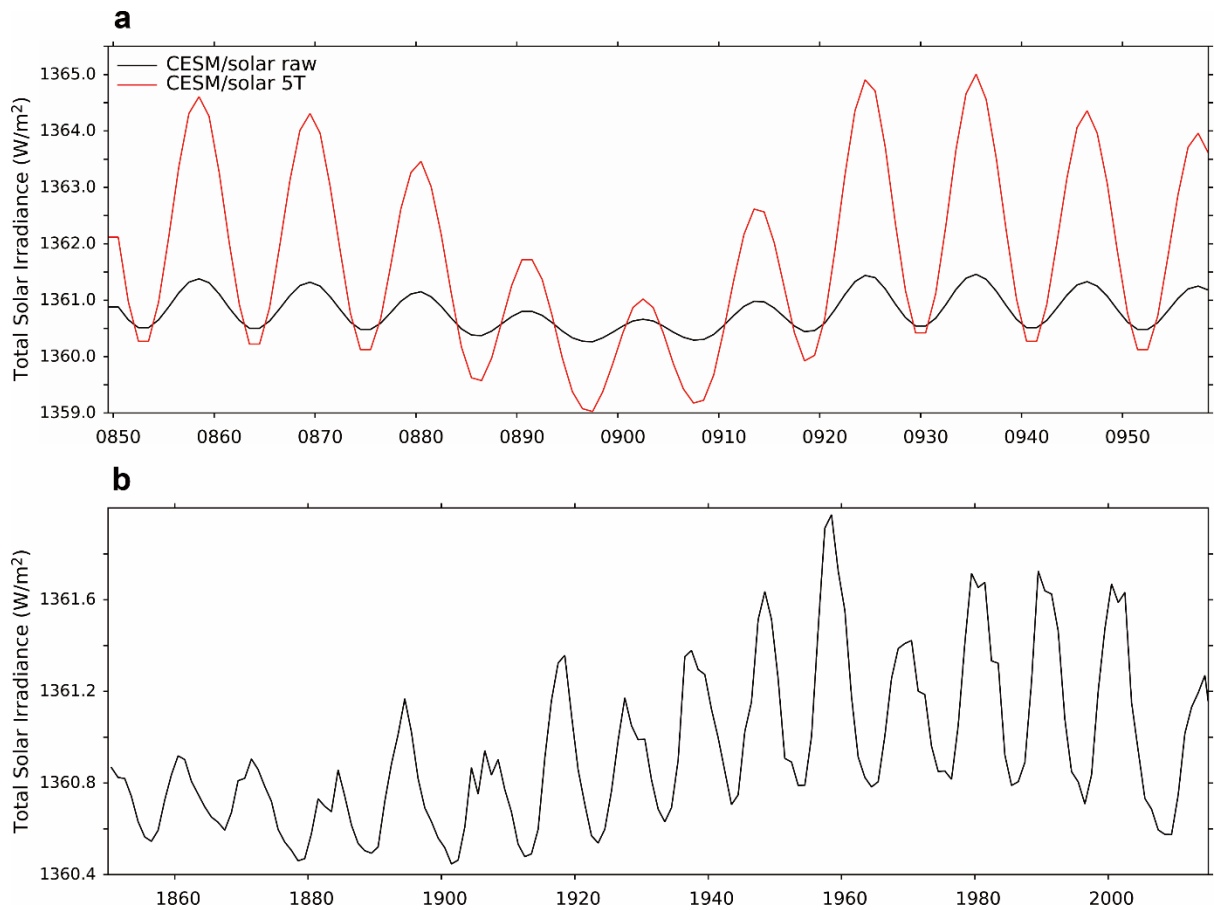
Supplementary Figure 7. Atmospheric responses in the North Pacific to the solar cycle during typhoon off-season (November to April) during the period 1948-2018.

Colors indicate regressions of off-season (November-April) (a) vertical wind shear (unit in m/s), (b) 850-hPa relative vorticity (unit in 10^{-6} 1/s), and (c) dynamic genesis potential index (DGPI) onto yearly normalized SSN at a one-year lag (i.e., SSN leads by one year). The stippled areas indicate where the regressions are significant at the 90% confidence level determined using a Student's t-test. The black boxes indicate the OMDR.



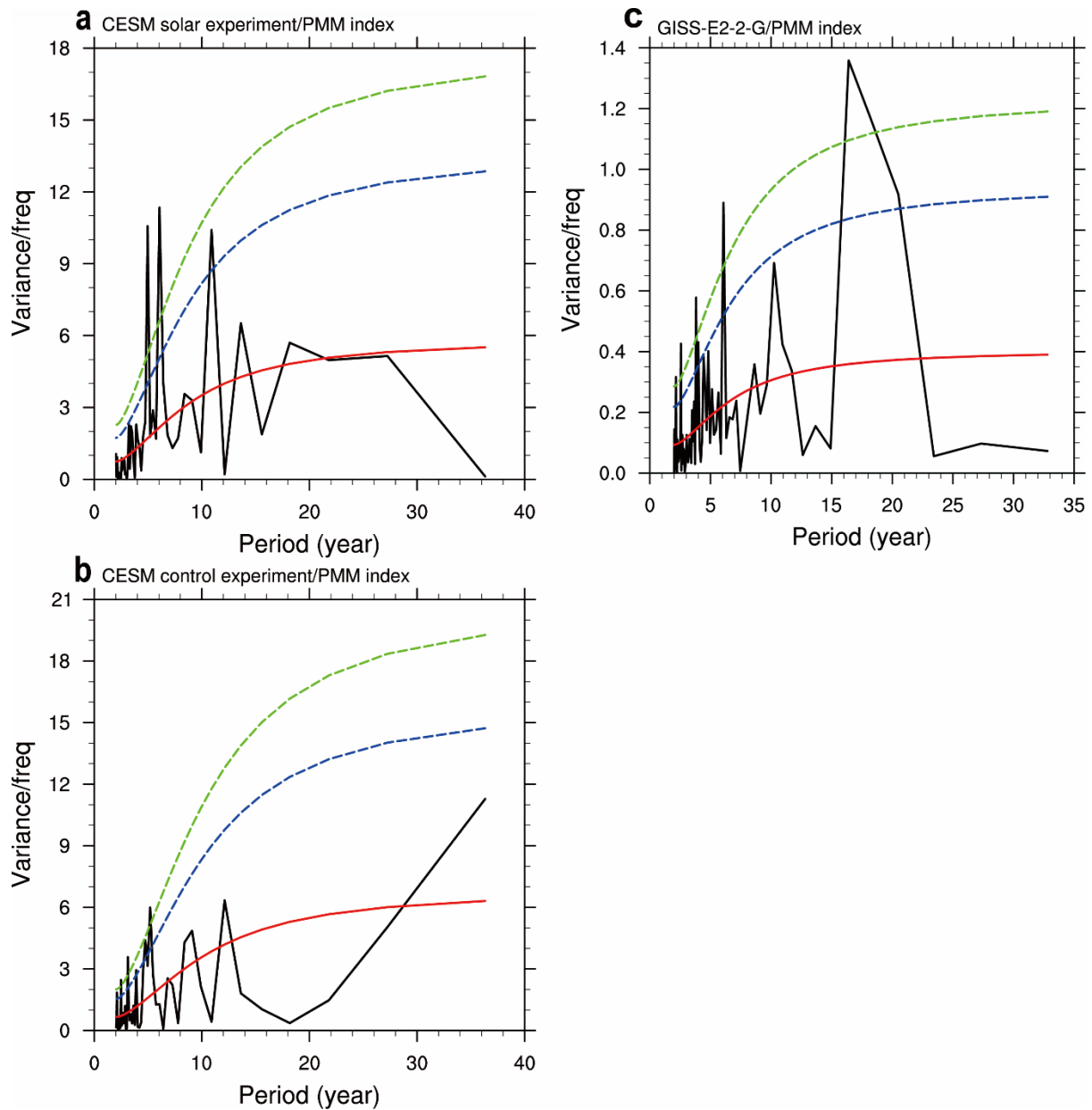
Supplementary Figure 8. Atmospheric circulation responses to solar forcing during the period 1948-2018.

Regressions of the off-season (November to April) (a) Northeastern Pacific (NEP, 180°W-100°W) mass streamfunction (colors, unit in 10^{11} kg/s) and (b) sea level pressure (colors, unit in hPa) and 850-hPa wind (arrows colors, unit in m/s) onto the yearly normalized SSN at a one-year lag (i.e., SSN leads by one year) during the period 1948-2018. The black boxes in (b) indicate the OMDR. The stippled areas indicate where the regressions are significant at the 90% confidence level determined using a Student's t-test.



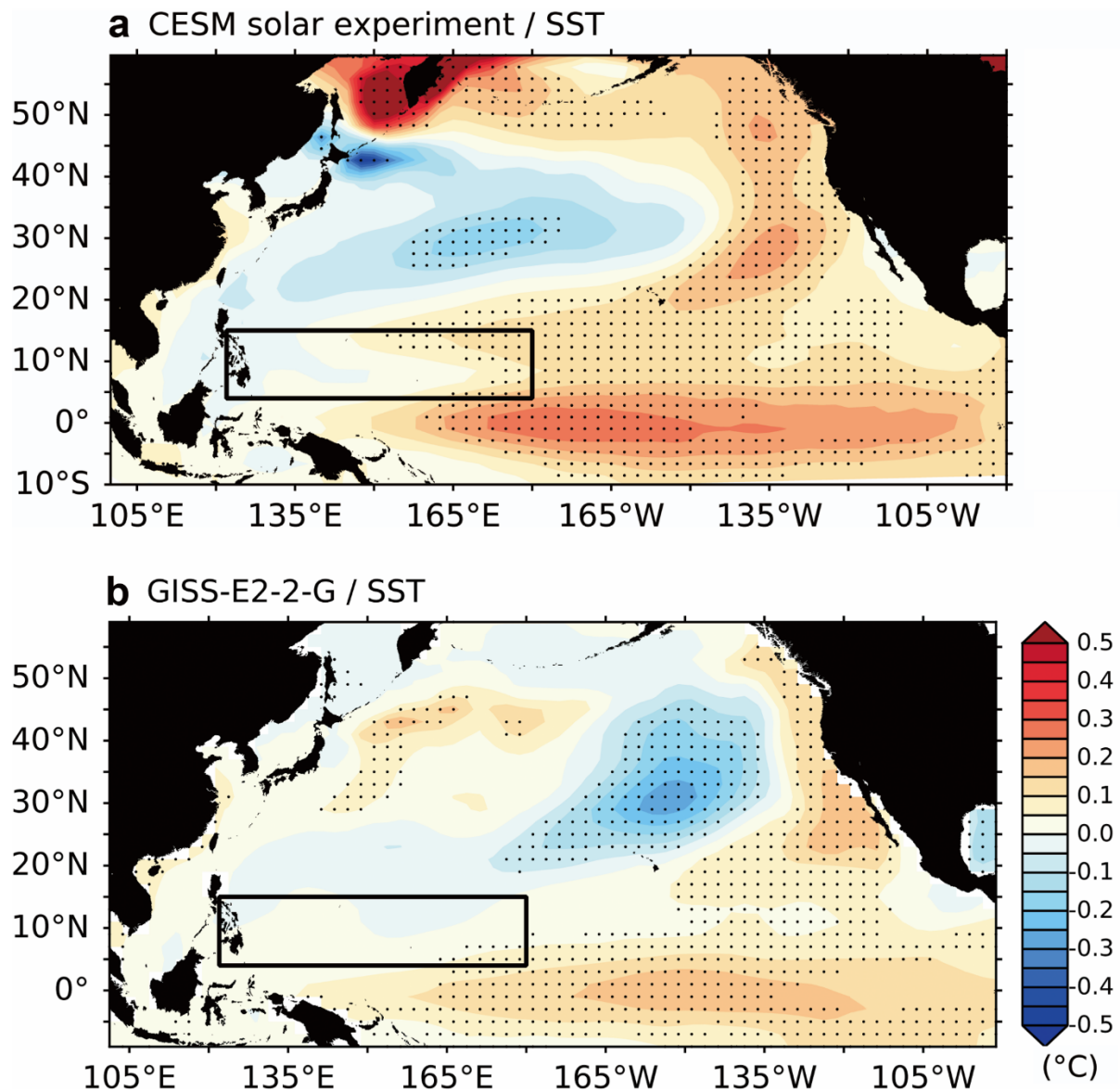
Supplementary Figure 9. Total Solar Irradiance time series used in the solar experiment with the CESM1 and CMIP6.

(a) The black line is the raw irradiance data observed from AD850 to AD950, which was amplified five times (red line) when used as forcing in the solar experiment with the CESM1 model. (b) same as (a), but for the irradiance forcing used in the GISS-E2-2-G historical-solar experiment.



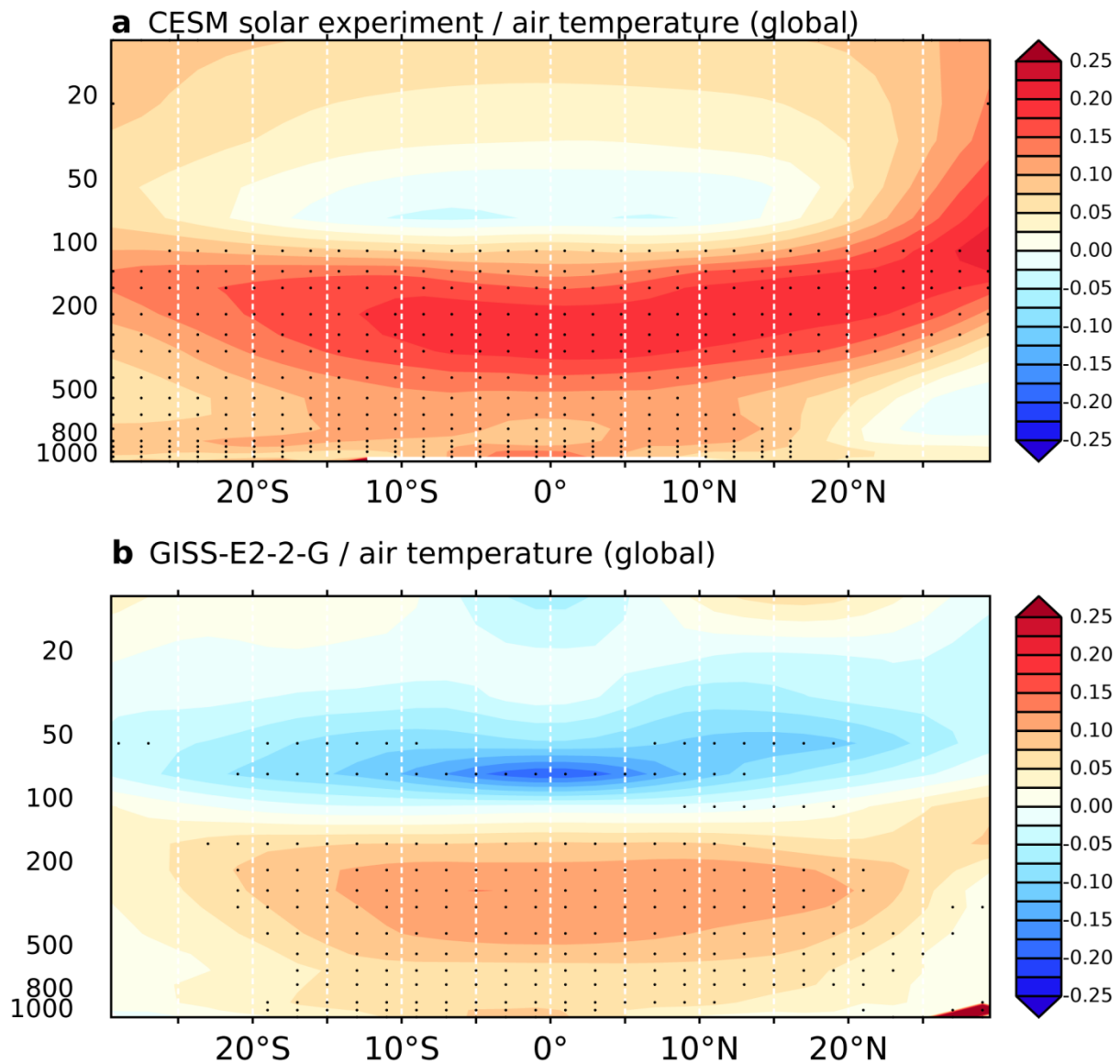
Supplementary Figure 10. Power spectrum of the off-season (November-April) PMM index in the idealized pair of the CESM1 solar experiments and GISS-E2-2-G historical-solar experiment

Power spectrum of the off-season PMM index (a) in the CESM1 solar experiment and (b) control experiment. (c) Same as (a), but for the GISS-E2-2-G historical-solar experiment. As an indicator of significance, a theoretical Markov red noise spectrum (red line) is displayed in all figures, with its 90th and 95th percentiles indicated by blue and green dashed lines, respectively.



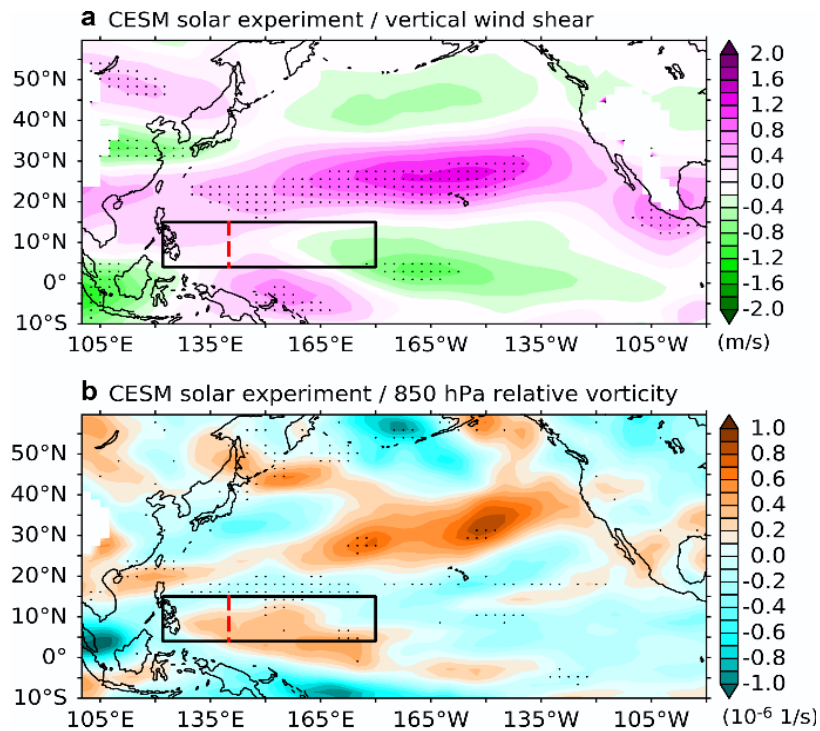
Supplementary Figure 11. The response of sea surface temperature (SST) in the North Pacific to the solar cycle prescribed in the CMIP6 and CESM1 solar experiment.

(a) Regressions of off-season (November-April) SST (colors, unit in °C) onto the yearly normalized Total Solar Irradiance (TSI; also see Fig. S9a) at a one-year lag (i.e., TSI leads by one year) for the solar experiment. (b) same as (a), but for regressions onto the yearly normalized Total Solar Irradiance (shown in fig. S9b) in the GISS-E2-2-G historical-solar experiment. The stippled areas indicate where the regressions are significant at the 90% confidence level determined using a Student's t-test. The black boxes denote the OMDR.



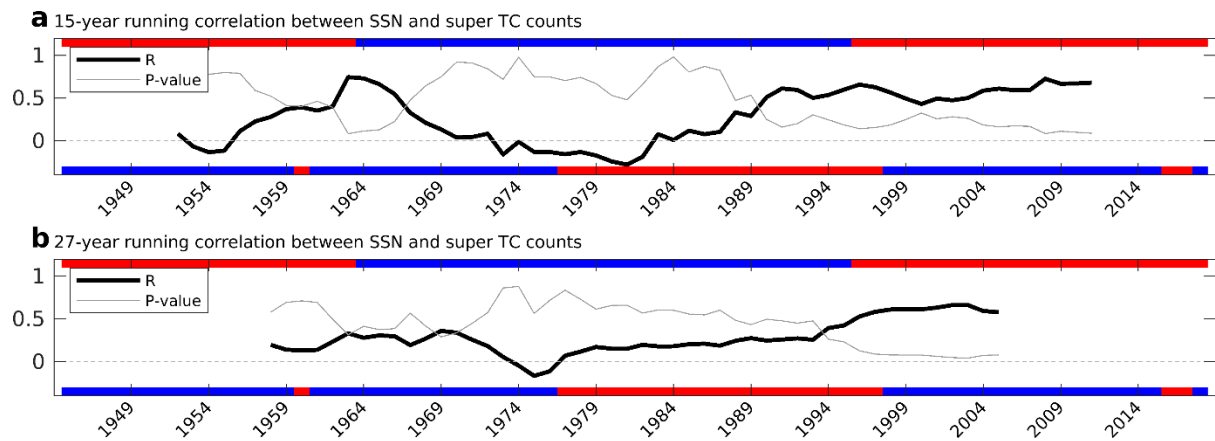
Supplementary Figure 12. The response of atmospheric temperature to the solar cycle prescribed in the CMIP6 and CESM1 solar experiment.

(a) Regressions of off-season (November-April) zonal-mean air temperatures ($^{\circ}\text{C}$) onto the yearly normalized Total Solar Irradiance (TSI; also see Fig. S9a) prescribed in the CESM1 solar experiment. (b) same as (a), but for regressions onto the yearly normalized Total Solar Irradiance (shown in fig. S9b) in the CMIP6 GISS-E2-2-G historical-solar experiment. The stippled areas indicate regressions that are significant at the 90% confidence level determined using a Student's t-test.



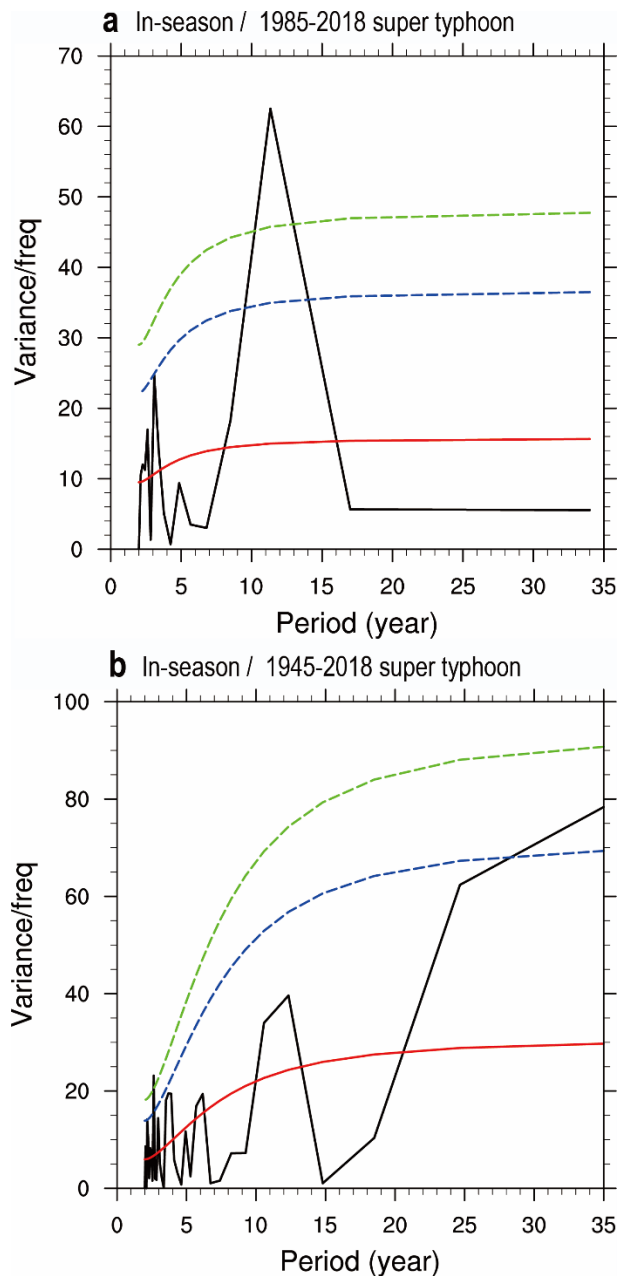
Supplementary Figure 13. The atmospheric responses to the solar cycle in the CMIP6 and CESM1 solar experiment.

Regressions (colors) of off-season (November-April) (a) vertical wind shear (unit in m/s), and (b) 850-hPa relative vorticity (unit in 10^{-6} 1/s) onto the yearly normalized Total Solar Irradiance (TSI; also see Fig. S9a) at a one-year lag (i.e., TSI leads by one year) for the CESM1 solar experiment. The stippled areas indicate where the regressions are significant at the 90% confidence level determined using a Student's t-test. The black boxes indicate the OMDR.



Supplementary Figure 14. The 15-year and 27-year running correlations between the yearly SSN and the number of off-season super typhoons at a one-year lag.

(a) The 15-year running correlation between the yearly SSN and the number of off-season super typhoons at a one-year lag (i.e., SSN leading the typhoon number by one year) is displayed using the black line for the correlation coefficient and gray line for the P-value. (b) same as (a), but for 27-year running correlation. The red and blue shadings at the top and bottom of all figures respectively indicate the positive and negative phases of the Atlantic Multi-decadal Oscillation (AMO) and Pacific Decadal Oscillation (PDO) determined using index values obtained by applying a 7-year running mean.



Supplementary Figure 15. Power spectrum of the yearly number of in-season (May-October) super typhoons in the western North Pacific.

(a) Power spectrum of the yearly number of in-season super typhoons in the western North Pacific during the period 1985-2018. (b) same as (a), but for the period 1945-2018. As an indicator of the significance of the spectrum, a theoretical Markov red noise spectrum (the red lines) is shown with its 90th and 95th percentiles indicated by blue and green dashed lines, respectively.